FURTHER EVIDENCE OF THE PLANETARY NATURE OF HD 95086 b FROM GEMINI/NICI *H*-BAND DATA

T. Meshkat[1], V. Bailey[2], J. Rameau[3], M. Bonnefoy[4], A. Boccaletti[5], E. E. Mamajek[6], M. Kenworthy[1],
G. Chauvin[3], A.-M. Lagrange[3], K. Y. L. Su[2], and T. Currie[7]

[1] Sterrewacht Leiden, P.O. Box 9513, Niels Bohrweg 2, 2300 RA Leiden, The Netherlands
[2] Steward Observatory, Department of Astronomy, University of Arizona, 933 North Cherry Avenue, Tucson, AZ 85721-0065, USA
[3] UJF-Grenoble 1/CNRS-INSU, Institut de Planétologie et d'Astrophysique de Grenoble (IPAG) UMR 5274, Grenoble, F-38041, France
[4] Max Planck Institute für Astronomy, Königsthul 17, D-69117 Heidelberg, Germany
[5] LESIA, Observatoire de Paris, CNRS, University Pierre et Marie Curie Paris 6 and University Denis Diderot Paris 7, 5 place Jules Janssen, F-92195 Meudon, France
[6] Department of Physics and Astronomy, University of Rochester, Rochester, NY 14627-0171, USA
[7] Department of Astronomy and Astrophysics, University of Toronto, 50 St. George St., Toronto, Ontario, M5S 1A1, Canada

ABSTRACT

We present our analysis of the Gemini/NICI *H*-band data of HD 95086, following the discovery of the planet HD 95086 b in L'. The *H*-band data reach a contrast of 12.7 mag relative to the host star at 5σ levels in the location of HD 95086 b, and no point source is found. Our non-detection and $H - L'$ color limit rules out the possibility that the object is a foreground L/T dwarf and that, if it is bound to HD 95086, it is a genuine planetary mass object. We estimate a new pre-main-sequence isochronal age for HD 95086 of 17 ± 4 Myr, which is commensurate with previous mean age estimates for the Lower Cen-Crux subgroup. Adopting an age of 17 Myr, the color limit is inconsistent with the COND model, marginally consistent with the BT-SETTL model, and consistent with the DUSTY model.

1. INTRODUCTION

Rameau et al. (2013) reported the probable detection of a 4 to 5 Jupiter mass companion to HD 95086 lying at a projected separation of 56 AU. The host is a young (17 ± 4 Myr; see Section 4.1) A8 type star. The large infrared excess (Chen et al. 2012) suggests that the star is harboring a debris disk, as yet unresolved.

The discovery at the L' band (3.8 μm), using the angular differential imaging technique (ADI; Marois et al. 2006), was a 9σ detection in the first epoch. The second epoch suffered from poor observing conditions, resulting in a 3σ re-detection of the planet. The astrometric precision allowed for the rejection of a background object with nearly 3σ probability. Rameau et al. (2013) also carried out Ks (2.18 μm) observations that also suffered from bad observing conditions. This resulted in low Ks sensitivity and a non-detection. These observations were used to conclude that the detection at L' was likely inconsistent with a background star. Such a non-detection rejected the background hypothesis and suggested a red object with $Ks - L' > 1.2$ mag.

With a predicted temperature of $T_{\rm eff} \simeq 1000$ K (compared to the 1600–1700 K of β Pic b, and 800–1100 K for HR8799 bcde; Bonnefoy et al. 2013; Currie et al. 2011; Skemer et al. 2012), a giant planet will have an atmosphere close to the L-T spectral transition, where the effect of reduced surface gravity (characteristic of young and low-mass companions) is expected to dramatically affect the balance between dust formation and settling in the atmosphere (Stephens et al. 2009). If the companion is real, it would be a benchmark for spectroscopic studies of low-mass giant planets since it would be one of the lightest directly imaged planets,[8] and key to testing predictions

about dust settling in low-gravity atmospheres. The methane bands seen in mature brown-dwarfs at a similar temperature as HD 95086 b might also be reduced (or lacking) due to the effect of reduced surface gravity, which in turn triggers non-equilibrium chemistry of CO/CH$_4$ (Hubeny & Burrows 2007).

Low-resolution spectroscopy is highly challenging with the present instrumentation given the contrast and faintness of HD 95086 b (Vigan et al. 2012). Broad band photometry is currently the only way to derive of the color of the companion and constrain its atmospheric properties. We examine our *H*-band NICI data[9] taken in 2012, the same epoch as the L' discovery image. We do not detect the companion in our *H*-band data, allowing us to derive a lower limit to the $H - L'$ color and reject a foreground contamination hypothesis.

In Sections 2 and 3, we describe our observations and our derived upper *H*-band limit. In Section 4, we discuss the age as determined by isochrone fitting and we show that the very red color rejects the foreground contamination hypothesis.

2. OBSERVATIONS

2.1. Data

Observations of HD 95086 were taken on UT 2012 March 19, 26, and 30 using the NICI camera (Toomey & Ftaclas 2003) on Gemini South in the *H*-filter ($\lambda = 1.65\,\mu$m and $\Delta\lambda = 0.29\,\mu$m) as part of a survey looking for gas giant planets around young stars with IR excesses (PI: V. Bailey). The camera was configured with the broad *H* band filter and the 0″.32 coronagraphic mask. The integration times for individual science frames are 55.0 s (5 coadded readouts of 11.0 s each). The details of the observing log for these data is listed in Table 1. Five percent of the frames are rejected per night due to poor alignment of the central star under the mask. The instrument was configured in telescope

---

[8] HR8799 b (Marois et al. 2008) might be as light as HD 95086 b but its low mass estimate was derived from dynamical instability rather than from atmospheric models which give higher mass, and Fomalhaut b might be a dwarf planet and only the reflecting dust is detected (Kalas et al. 2008; Currie et al. 2012).

[9] Taken as part of a survey of young stars with debris disks (PI: V. Bailey).

Table 1
Observing Log for NICI *H*-band 2012 Data

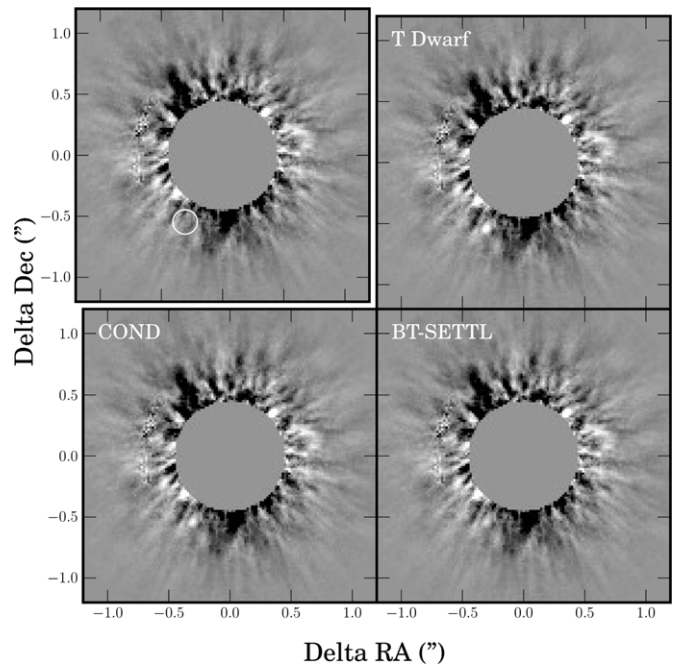| Date (UT)	2012 Mar 19	2012 Mar 26	2012 Mar 30
Total integration time (s)	2695	3520	3520
Frames observed	49	64	64
Frames rejected	5	4	4
On-sky rotation (°)	18.24	25.13	25.19
Parallactic angle (°)	18.89/37.13	342.14/07.27	347.71/12.90
DIM seeing (″)	0.6	0.6	0.6

Figure 1. Upper left: the combined NICI *H*-band image reduced with PCA with a white circle at the expected location of the companion. The three other images have a fake companion injected into the raw data at the location of the expected planet. The contrast of the artificial companions are 11.6 mag for the T dwarf, 12.0 mag for the COND model, and 12.5 mag for the BT-SETTL model.

pupil tracking mode to keep the point spread function (PSF) structure from the telescope optics fixed with respect to the orientation of the detector. As a consequence, the position angle (P.A.) of the sky on the detector underwent rotation of 19°, 25°, and 25° on each of the nights, respectively.

2.2. NICI Data Reduction

Calibration data consists of dark frames with the same integration time and flats from the nights of March 19 and 26. The flat field images were dark-subtracted, and all individual flat field images were normalized by their median and combined together with a clipped mean to form a final normalized flat field image.

The dark frames were subtracted from the science frames and then the dark-subtracted science frames were divided by the normalized flat field frame. A bad pixel mask was constructed from pixels in the flat field frame that were greater than 1.2 or less than 0.8 in value. These bad pixels were interpolated over using adjacent good values in the science frames. Hot, cold, and flaky pixels were found and interpolated over in individual science frames by their values being more than 1000 counts different from the median of a 3×3 box centered on that pixel. Finally, the NICI distortion correction was applied to the images in order to perform astrometry on the additional background sources in the field of view.

2.3. Photometric Calibration

Due to the radial transmission function of the apodizer (Wahhaj et al. 2011) and the level of adaptive optics correction on the central star, photometric calibration was performed using a background star visible 4″.5 away from the primary star in the images. It was first detected by Kouwenhoven et al. (2005) and confirmed as a background object by Rameau et al. (2013). This background star was used as a photometric reference to determine the flux calibration and sensitivity in our *H*-band data. The NICI coronagraphic transmission curve is not yet published, thus to determine the near-infrared photometry of the background star, we utilize archival photometry from *Hubble Space Telescope* (*HST*) NICMOS data taken in 2007 (program 11157, PI: Joseph Rhee). The calibrated mosaic files provided by the *HST* archive are background-subtracted and normalized by exposure time. Two images, one per roll angle, are taken in each F110W and F160W; each of the four images has a total exposure time of 895 s. We roll-subtracted each pair of images, and used the aperture diameter and corresponding aperture correction recommended by the NICMOS data reduction handbook for NIC2. We derived the magnitudes in F110W and F160W of 13.63 ± 0.05 and 12.81 ± 0.05 for the background star. We used the transformations of Stephens et al. (2000) to derive *J* and *H* magnitudes of 13.25 ± 0.10 and 12.81 ± 0.10, respectively.

3. IMAGE PROCESSING

The data were centroided in a smaller frame which ensured the background visual binary star is clearly visible at an angular separation of 4″.5 and a P.A. of 330°. The unsaturated visual binary star is crucial for photometry, as the host star was blocked by the coronagraph, and the transmission of the light from the star is not well constrained. Kouwenhoven et al. (2005) estimated this star to have a *Ks* magnitude of 12.67 mag. Rameau et al. (2013) found the background star to have a $Ks - L'$ color of -0.3 ± 0.2 mag. Using our NICMOS-derived *H*-band magnitude of the background star, we estimate a $H - Ks$ color of 0.14 ± 0.10 mag for the background star.

To understand the impact of imaging processing on the detectability of faint sources, we processed the data with artificially added planets with three independent pipelines: one by Meshkat et al. (2013) based on principal component analysis (PCA) (Amara & Quanz 2012), one by Boccaletti et al. (2013) using locally optimized combination of images (LOCI) (Lafrenière et al. 2007), and one by Chauvin et al. (2012) using ADI. The three pipelines agree with each other, and here we only show the results using PCA.

The PCA pipeline was run separately for the data from each night, with an inner radius of 0″.50 corresponding to the edge of the coronagraphic mask. For each dataset, five principal components were used to create a model of the stellar coronagraphic image. This optimal number of principal components was determined by injecting artificial components at the same angular separation with a different P.A. from the expected planet. The final de-rotated datacubes from each night are averaged for a final image.

Figure 1 shows the PCA reduced image in the upper left corner. No point sources are seen at the expected position (see the white circle in Figure 1). The other images are with an artificial planet injected with the contrast and angular separation
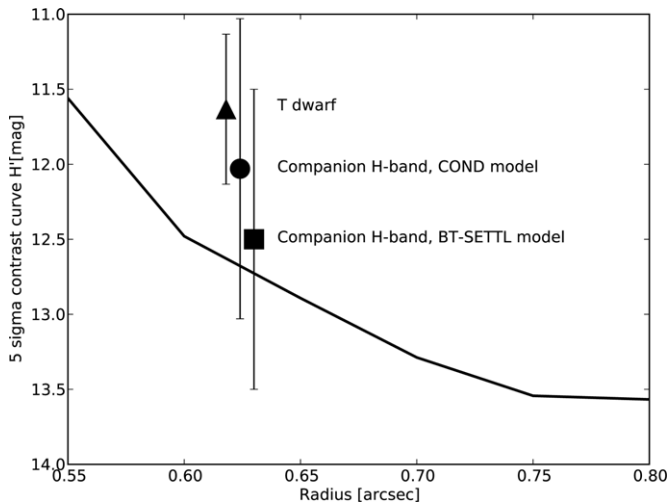
Figure 2. Contrast curve for *H*-band NICI data on HD 95086 generated by injecting artificial planets in the three nights of data. The circle, square, and triangle indicate the expected *H*-band contrast for a 17 Myr COND model planet, BT-SETTL model planet, and T dwarf, respectively. The square and triangle are slightly offset from the expected angular separation (0″624) for clarity.

(0″624) of the expected companion if it were a T dwarf (11.6 mag), COND model planet (12.0 mag), and BT-SETTL model planet (12.5 mag) (for details see Section 4.2).

We injected artificial sources in all three nights of data combined to determine the 5σ detection limit. The background star was used to generate the artificial planets by rescaling the flux to between 10 and 14 mag fainter than the primary star, from 0″55 to 0″8 in 0″05 increments.

The signal-to-noise (S/N) of the resulting fake planet is determined by the following equation:

$$(S/N)_{\text{planet}} = \frac{F_{\text{planet}}}{\sigma(r)\sqrt{\pi r_{\text{ap}}^2}}$$

where F_{planet} is the sum of the flux in an aperture with a radius, r_{ap}, of 2 pixels, σ is the root mean square of the pixels in a 340° arc at the same radius around the star (excluding the planet itself), and r is the width of the arc (2 pixels). We can then construct the distribution of S/N at various source magnitudes, and determine the 5σ detection limit by interpolation at a given radius from the star. The 5σ contrast curve is shown in Figure 2.

To make sure the source brightness is not affected by the NICI coronagraph, we extrapolated the transmission measured in the CH$_4$ filter (Boccaletti et al. 2013), assuming a linear relation with wavelength, and concluded that it should have nearly 100% transmission at greater than 0″6. Since the planet is detected at a separation of 0″624, this is within the 100% transmission regime.

4. ANALYSIS

4.1. Stellar Parameters and Age

HD 95086 was kinematically selected as a member of Lower Cen-Crux (LCC) based on its *Hipparcos* astrometry by de Zeeuw et al. (1999), and it has been included in several later studies as a member (e.g., Rizzuto et al. 2012; Chen et al. 2012). The *mean* age of the LCC subgroup defined by the >1 $M_{\odot}$ stars is ∼16–17 Myr, however, the inferred age spread of the group (∼10 Myr) hints that adoption of the mean subgroup
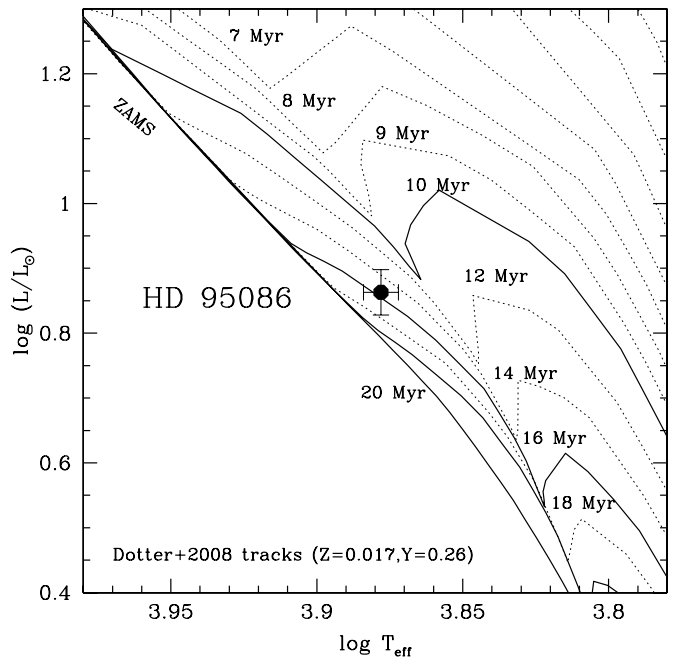

Figure 3. H-R diagram for HD 95086 with Dartmouth isochrones overlaid.

age for a given star may be problematic (Mamajek et al. 2002; Preibisch & Mamajek 2008; Pecaut et al. 2012). The revised *Hipparcos* astrometry for the star from van Leeuwen (2007) differs negligibly from the original value, and indeed Rizzuto et al. (2012) again included HD 95086 in a recent analysis, so we regard the kinematic membership as secure.

The *Hipparcos* catalog quotes photometry of $V = 7.36$ and $B - V = 0.230 \pm 0.004$. If the intrinsic colors of HD 95086 are similar to that of A8V dwarf stars, then their mean color is $B - V = 0.25$ (Pecaut & Mamajek 2013), with an rms spread of ±0.04 mag. This is not surprising, as low reddening values ($E(B - V) < 0.05$ mag) are ubiquitous for stars within 90 pc in the general direction of HD 95086 (Reis et al. 2011). Based on this discussion, we adopt $A_V = 0.02 \pm 0.02$ mag as a reasonable estimate that brackets the range of plausible extinctions and confirm the spectral type discussion in Rameau et al. (2013).

We calculate an absolute magnitude of $M_V \simeq 2.6$, which places the star near the main sequence (MS). The combined constraints of spectral type A8 ±1 (assumed uncertainty) and restricting the plausible reddening value to be $E(B - V) < 0.05$ leads to an effective temperature estimate of 7550 ± 100 K ($\log(T_{\text{eff}}) = 3.878 \pm 0.006$) and *V*-band bolometric correction of $BC_V = 0.040 \pm 0.002$ mag (statistical) ±0.026 mag (systematic), where the systematic uncertainty reflects differences in the bolometric magnitude scales among six studies (Code et al. 1976; Balona 1994; Flower 1996; Bessell et al. 1998; Bertone et al. 2004; Masana et al. 2006). Combining the *Hipparcos V* magnitude (assuming ±0.01 mag uncertainty), the revised *Hipparcos* parallax, and our stated extinction and bolometric magnitude values, we estimate the following parameters for HD 95086: apparent bolometric flux $f_{\text{bol}} = 28.52 \pm 0.9$ pW m^{-2}, absolute *V* magnitude $M_V = 7.38 \pm 0.03$, absolute bolometric magnitude 2.60 ± 0.09, $\log(L/L_{\odot}) = 0.863 \pm 0.035$ dex.

In Figure 3, we plot the H-R diagram point for HD 95086 with Dartmouth isochrones from Dotter et al. (2008) adopting approximately protosolar composition of $Y = 0.26$ and $Z = 0.017$. The star is slightly above the zero-age main sequence

(ZAMS), and appears consistent with pre-MS age 16 ± 2 Myr. Using three other sets of pre-MS evolutionary tracks, we find the following ages: 15 Myr (D'Antona et al. 1997), 17 Myr (Yi et al. 2003), and 24 Myr (Siess et al. 1997). Note that models are in general agreement on the mass of HD 95086: $\sim$1.7 $M_\odot$. Taking into account the different models and observational uncertainties, we estimate a final individual pre-MS isochronal age estimate of HD 95086 of 17 Myr ($\pm$2 Myr statistical, $\pm$4 Myr systematic, total uncertainty $\sim\pm$4 Myr). This is commensurate with the mean LCC subgroup age (Mamajek et al. 2002; Pecaut et al. 2012).

Two factors which could conspire to ruin our age estimate are (1) unresolved binarity (which would move the star older, closer to the ZAMS), and (2) if the star is an interloper whose H-R diagram position and kinematics could conspire to masquerade the star appear as a likely LCC member. In the unlikely scenario that the star is an interloper, its H-R diagram position would be consistent with an MS isochronal age of $\sim$270 Myr.

4.2. Color Constraints

At the angular separation of the planet ($0''.624$), we are sensitive to an H-band contrast of 12.7 mag relative to the host star for a 5σ point source detection. This is an apparent magnitude of 19.57 mag. Using the Rameau et al. (2013) apparent L' magnitude of 16.49, we derive an $H - L'$ lower limit of 3.1 ± 0.5 mag for the planet at 5σ.

The expected H-band contrast of the planet, given the measured L' magnitude (Rameau et al. 2013), is 12.03 ± 1.0 mag based on the COND model (Baraffe et al. 2003) and 12.50 ± 1.0 mag based on the BT-SETTL model (Allard et al. 2013; Figure 2). The error is propagated from the uncertainty in the L' magnitude in Rameau et al. (2013). The contrast curve demonstrates that our data are sensitive enough to detect a planet for the COND models ($S/N > \sim$4) and the BT-SETTL models ($S/N > \sim$2.5). Instead, we detect no point sources at such brightness in our H-band data.

The expected H magnitudes for an unreddened A/F star, M dwarf, and T dwarf interlopers which are at the same distance as HD 95086 are 16.5, 17.5, and 18.5 (see triangle, Figure 2), respectively. This is far brighter than our 19.57 detection limit at the angular separation of the companion. If the companion were a T dwarf at the distance of HD 95086 or closer, we would have seen it based on our color and sensitivity limits. An unreddened K giant would have to be at 40 kpc in order to have the same L' magnitude as the companion, and its $H - L'$ color would be 0.17, which we would have detected. The companion is very unlikely to be a background source due to the proper motion seen in Rameau et al. (2013).

We compared the constraints on the photometry of HD 95086 b (shaded area) in a color–magnitude diagram (Figure 4) to the photometry of field M, L, and T dwarfs (Leggett et al. 2013), of young (12–30 Myr) companions (HR7329 B, Neuhäuser et al. (2011); Kappa And b, Carson et al. (2013), Bonnefoy et al. (2013); β Pic b, Lagrange et al. (2010), Bonnefoy et al. (2013); 2M0103 ABb, Delorme et al. (2013); AB Pic b, Chauvin et al. (2005); 2M1207 b, Chauvin et al. (2004); HR8799 bcde, Marois et al. (2008), Skemer et al. (2012), and to the COND model, the DUSTY model Chabrier et al. (2000), and the BT-SETTL model generated for an age of 17 Myr. The $H - L'$ color of HD 95086 b makes it one of the reddest companions directly imaged so far. It is inconsistent with COND models, consistent with 4–5 $M_{\rm Jup}$ BT-SETTL models, and consistent DUSTY models at an age of 17 Myr. The color is also at least
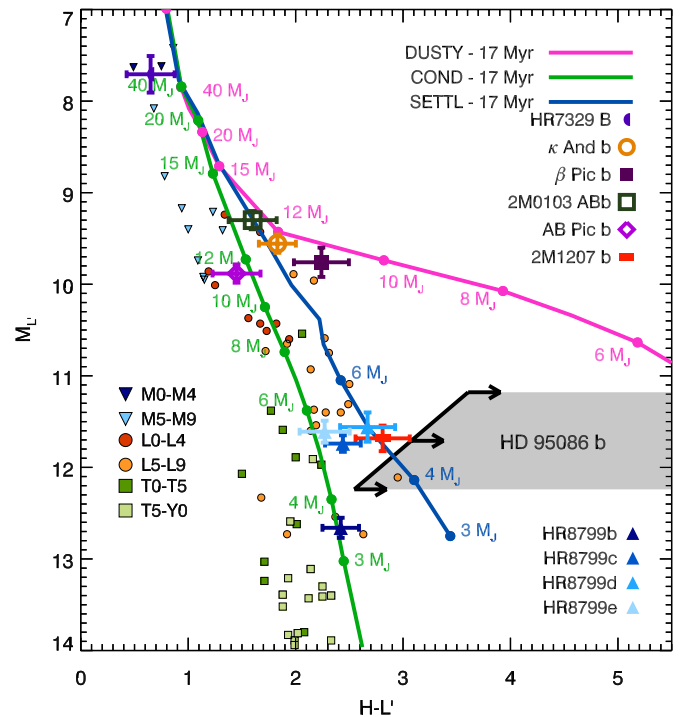

Figure 4. Color–magnitude diagram showing the $M_{L'}$ vs. $H - L'$ color of various substellar objects as well as tracks from evolutionary and atmospheric models. The shaded area is defined as a lower limit on the color of the HD 95086 companion.

(A color version of this figure is available in the online journal.)

2 mag redder than the ones of typical M field dwarfs and 1 mag redder than the colors of early-L dwarfs. The location of the companion with respect to the sequence of field brown dwarfs and to evolutionary tracks suggest a high dust content in its photosphere (possibly under the form of thick clouds; Currie et al. 2011). In summary, current constraints on the photometry of HD 95086 b further suggest that the source is likely a bound companion with peculiar atmospheric properties related to low surface gravity. A new astrometric epoch is still mandatory to confirm that the companion is comoving with the star, and then exclude the possibility that it could be an extincted or intrinsically red background or foreground object.

4.3. Proper Motion of Background Sources

There are 20 additional point sources visible in the H-band distortion corrected images, ranging from $2''$ to $10''$ away from HD 95086. Using NICMOS *HST* data from 2007 (PI: J. Rhee), we examine the proper motion of these sources relative to HD 95086 with a five-year baseline. The proper motion of all the point sources in the field of view are consistent with background sources.

5. CONCLUSION

We analyze H-band NICI data aiming to re-detect the planet HD 95086 b. We detect no point source in our data, verified through three independent pipelines. Our deep dataset provides an $H - L'$ lower limit, which rules out foreground L/T dwarfs and distant background K giant contaminants. If the object is bound to HD 95086, our color limit is inconsistent with the COND model, marginally consistent with the BT-SETTL model, and consistent with the DUSTY model at our derived age of 17 ± 4 Myr. Future astrometric observations are necessary

to establish the nature of this object. This extremely red object demonstrates the importance of L' band for planet detection as planets may be much redder than models predict.

REFERENCES

Allard, F., Homeier, D., Freytag, B., Schaffenberger, W., & Rajpurohit, A. S. 2013, Memorie della Societa Astronomica Italiana Supplementi, 24, 128

Amara, A., & Quanz, S. P. 2012, MNRAS, 427, 948

Balona, L. A. 1994, MNRAS, 268, 119

Baraffe, I., Chabrier, G., Barman, T. S., Allard, F., & Hauschildt, P. H. 2003, A&A, 402, 701

Bertone, E., Buzzoni, A., Chávez, M., & Rodríguez-Merino, L. H. 2004, AJ, 128, 829

Bessell, M. S., Castelli, F., & Plez, B. 1998, A&A, 333, 231

Boccaletti, A., Lagrange, A.-M., Bonnefoy, M., Galicher, R., & Chauvin, G. 2013, A&A, 551, L14

Bonnefoy, M., Boccaletti, A., Lagrange, A.-M., et al. 2013, A&A, 555, A107

Bonnefoy, M., Currie, T., Marleau, G.-D., et al. 2013, A&A, in press (arXiv:1308.3859)

Carson, J., Thalmann, C., Janson, M., et al. 2013, ApJL, 763, L32

Chabrier, G., Baraffe, I., Allard, F., & Hauschildt, P. 2000, ApJ, 542, 464

Chauvin, G., Faherty, J., Boccaletti, A., et al. 2012, A&A, 548, A33

Chauvin, G., Lagrange, A.-M., Dumas, C., et al. 2004, A&A, 425, L29

Chauvin, G., Lagrange, A.-M., Zuckerman, B., et al. 2005, A&A, 438, L29

Chen, C. H., Pecaut, M., Mamajek, E. E., Su, K. Y. L., & Bitner, M. 2012, ApJ, 756, 133

Code, A. D., Bless, R. C., Davis, J., & Brown, R. H. 1976, ApJ, 203, 417

Currie, T., Burrows, A., Itoh, Y., et al. 2011, ApJ, 729, 128

Currie, T., Debes, J., Rodigas, T. J., et al. 2012, ApJL, 760, L32

D'Antona, F., Caloi, V., & Mazzitelli, I. 1997, ApJ, 477, 519

de Zeeuw, P. T., Hoogerwerf, R., de Bruijne, J. H. J., Brown, A. G. A., & Blaauw, A. 1999, AJ, 117, 354

Delorme, P., Gagné, J., Girard, J. H., et al. 2013, A&A, 553, L5

Dotter, A., Chaboyer, B., Jevremović, D., et al. 2008, ApJS, 178, 89

Flower, P. J. 1996, ApJ, 469, 355

Hubeny, I., & Burrows, A. 2007, ApJ, 669, 1248

Kalas, P., Graham, J. R., Chiang, E., et al. 2008, Sci, 322, 1345

Kouwenhoven, M. B. N., Brown, A. G. A., Zinnecker, H., Kaper, L., & Portegies Zwart, S. F. 2005, A&A, 430, 137

Lafrenière, D., Marois, C., Doyon, R., Nadeau, D., & Artigau, É. 2007, ApJ, 660, 770

Lagrange, A.-M., Bonnefoy, M., Chauvin, G., et al. 2010, Sci, 329, 57

Leggett, S. K., Morley, C. V., Marley, M. S., et al. 2013, ApJ, 763, 130

Mamajek, E. E., Meyer, M. R., & Liebert, J. 2002, AJ, 124, 1670

Marois, C., Lafrenière, D., Doyon, R., Macintosh, B., & Nadeau, D. 2006, ApJ, 641, 556

Marois, C., Macintosh, B., Barman, T., et al. 2008, Sci, 322, 1348

Masana, E., Jordi, C., & Ribas, I. 2006, A&A, 450, 735

Meshkat, T., Kenworthy, M., Quanz, S. P., & Amara, A. 2013, ApJ, submitted

Neuhäuser, R., Ginski, C., Schmidt, T. O. B., & Mugrauer, M. 2011, MNRAS, 416, 1430

Pecaut, M., & Mamajek, E. E. 2013, ApJ, in press (arXiv:1307.2657)

Pecaut, M. J., Mamajek, E. E., & Bubar, E. J. 2012, ApJ, 746, 154

Preibisch, T., & Mamajek, E. 2008, Handbook of Star Forming Regions, Vol. 2 (San Francisco, CA: ASP), 235

Rameau, J., Chauvin, G., Lagrange, A.-M., et al. 2013, ApJL, 772, L15

Reis, W., Corradi, W., de Avillez, M. A., & Santos, F. P. 2011, ApJ, 734, 8

Rizzuto, A. C., Ireland, M. J., & Zucker, D. B. 2012, MNRAS, 421, L97

Siess, L., Forestini, M., & Dougados, C. 1997, A&A, 324, 556

Skemer, A. J., Hinz, P. M., Esposito, S., et al. 2012, ApJ, 753, 14

Stephens, A. W., Frogel, J. A., Ortolani, S., et al. 2000, AJ, 119, 419

Stephens, D. C., Leggett, S. K., Cushing, M. C., et al. 2009, ApJ, 702, 154

Toomey, D. W., & Ftaclas, C. 2003, Proc. SPIE, 4841, 889

van Leeuwen, F. 2007, A&A, 474, 653

Vigan, A., Bonnefoy, M., Chauvin, G., Moutou, C., & Montagnier, G. 2012, A&A, 540, A131

Wahhaj, Z., Liu, M. C., Biller, B. A., et al. 2011, ApJ, 729, 139

Yi, S. K., Kim, Y.-C., & Demarque, P. 2003, ApJS, 144, 259